Quantum Electronics **50** (11) 1055–1062 (2020)

LASER APPLICATIONS AND OTHER ISSUES IN QUANTUM ELECTRONICS https://doi.org/10.1070/QEL17398

Lidar-based remote infrared gas sensor for monitoring anthropogenic pollution: a proof of concept

V.V. Meshcherinov, M.V. Spiridonov, V.A. Kazakov, A.V. Rodin

Abstract. **We propose using wavelength-modulation laser absorption spectroscopy in combination with quadrature detection of scattered light for remote industrial pollution monitoring in the atmosphere with a compact lidar-based gas sensor, which can be mounted on board an unmanned aerial vehicle. The instrument can be used for detecting leaks in product pipe lines; monitoring toxic gases near landfill sites, waste incineration plants, and other hazardous man-made facilities; analysing the gas atmosphere in industrial buildings and structures; and monitoring engineering processes at a sensitivity level of tens of ppm m in gas concentration measurements at characteristic distances of tens of metres.**

Keywords: *lidar, diode laser, modulation spectroscopy, quadrature detection, industrial pollution.*

1. Introduction

Detection of gaseous components of atmospheric air has a wide range of applications. In the petrochemical and processing industries, sensors for monitoring particular gases are used to ensure safety by detecting elevated concentrations of toxic or highly flammable gases [1]. High-sensitivity gas spectrometers are widely used in atmospheric studies for measuring vertical concentration profiles of individual gases, including greenhouse gases, and identifying their spread channels [2]. In medical applications, gas analysis can be used e.g. to diagnose the exhaled gas mixture [3].

Apparatus for quantitative analysis of atmospheric composition is dominated by laboratory analytical equipment, such as gas chromatographs, requiring preliminary sample preparation, which precludes real-time data acquisition, or Fourier transform spectrometers, which offer high spectral resolution, but have large dimensions and weight. One example of the use of commercial laboratory equipment for addressing global issues in gas sensing is the Total Carbon Column Observing Network (TCCON), a ground-based greenhouse gas emission monitoring system [4]. This international network of sites employs Bruker 125HR Fourier transform spectrometers operating in the near-IR spectral region, which allow one to determine various greenhouse gases in the atmosphere with high accuracy. Offering obvious advantages for laboratory investigations, instruments of this class are typically sensitive to external influences, have a large weight and large dimensions, and are expensive, which limits their utility for practical applications.

Among more compact and less expensive tools for gas detection, semiconductor gas sensors and electrochemical devices warrant attention. Semiconductor gas sensors are capable of detecting very low target gas concentrations [5], but they suffer from temporal drift and a cross-response to other gases, and their sensitivity depends on ambient humidity. Electrochemical gas sensors offer high selectivity for a target gas, with concentration measurement sensitivity levels down to a few ppm or ppb [6], but they have a limited service life and are also sensitive to humidity changes.

Another class of gas analysers take advantage of a selective optical absorption in a gaseous medium. Such instruments ensure a fast response, with a time constant less than 1 s, extremely low drift, and high gas selectivity, with the possibility of zero cross-response to other gases. Measurements can be performed in real time in active or passive mode [7]. In addition to cheap, low-performance sensors and laboratory-scale equipment, there are devices based on optical gas detection methods, which allow many practical issues to be resolved.

In applications related to environmental monitoring and protection, direct gas sampling is often impossible because of a large distance to the object, a large area of the territory to be examined, or high reactivity of the medium to be analysed. In such cases, it is expedient to use remote gas analysis methods, both passive, based on spectral analysis of natural emission from an object, and active, in which an object is illuminated in a preset spectral range and the transmitted or scattered light is analysed.

2. Remote laser gas analysis methods

A widespread remote optical gas analysis method is tunable laser absorption spectroscopy [8]. Owing to its high spectral resolution, which makes it possible to resolve the profile of individual rotational lines in rovibrational absorption spectra of molecular gases, this method is widely used in studies and

V.V. Meshcherinov Moscow Institute of Physics and Technology (National Research University), Institutskii per. 9, 141700 Dolgoprudnyi, Moscow region, Russia;
e-mail: meshcherinov@phystech.edu;
M.V. Spiridonov Moscow Institute of Physics and Technology (National Research University), Institutskii per. 9, 141700 Dolgoprudnyi, Moscow region, Russia; Prokhorov General Physics Institute (Federal Research Center), Russian Academy of Sciences, ul. Vavilova 38, 119991 Moscow, Russia;
V.A. Kazakov, A.V. Rodin Moscow Institute of Physics and Technology (National Research University), Institutskii per. 9, 141700 Dolgoprudnyi, Moscow region, Russia; Space Research Institute, Russian Academy of Sciences, Profsoyuznaya ul. 84/32, 117997 Moscow, Russia

Received 7 July 2020
Kvantovaya Elektronika **50** (11) 1055–1062 (2020)
Translated by O.M. Tsarev

diagnosis of substances in the gas phase. In addition to determining the gas composition in the zone of interest and the concentrations of individual gas components, a resolved profile of a spectral line offers the possibility of measuring the temperature, pressure, flow velocity, and other parameters of gaseous media [9, 10]. This method is of practical importance for engineering processes, safety issues, industrial emission analysis, and environmental monitoring.

Characteristic spectral lines corresponding to rovibrational transitions of many molecular gases of interest as markers of various natural photochemical or anthropogenic processes lie in the IR spectral region. Figure 1 shows spectral absorption lines of carbon dioxide and a number of minor atmospheric air components in the near- and mid-IR spectral regions, calculated with the use of the HITRAN database.

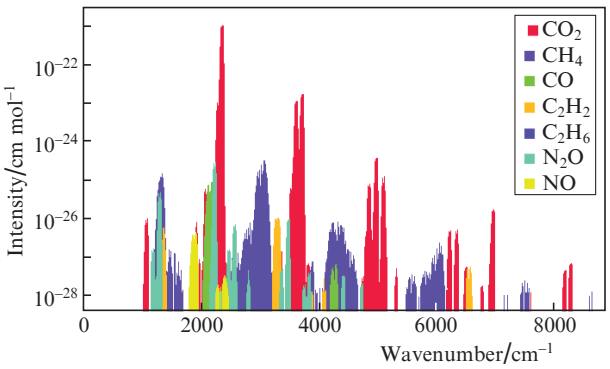

Figure 1. (Colour online) Spectral absorption lines of some molecular gases in the IR spectral region.

In this spectral range, wide use is made of quantum cascade and diode lasers [11]. To date, the mid-IR niche has been filled by commercial quantum cascade lasers, because they can function at room temperature without cryogenic cooling, and in some cases even without liquid cooling. Diode lasers emitting in the mid-IR spectral region are more demanding of cooling systems. At the same time, near-IR diode lasers offer excellent performance parameters, which allow them to be applied in absorption spectroscopy. Moreover, owing to the explosive growth in telecommunication technologies, the cost of the diode lasers that are used as light sources in the range 1.26–1.68 μm, as well as the cost of the optical fibre and photodetectors intended for operation in this range, has decreased significantly [12].

The spectral resolution of tunable laser absorption spectroscopy is determined in large measure by laser frequency stabilisation and tuning accuracy. Since Fabry–Perot lasers have a tendency toward mode hopping [13], spectroscopic applications rely predominantly on distributed feedback (DFB) semiconductor lasers, which ensure a narrow emission line (~1 MHz) and emission wavelength stability down to 10^{-4} cm^{-1}. In addition, their tuning range can reach 50 cm^{-1}. The emission wavelength of standard DFB lasers can be controlled by varying the temperature of the laser gain medium using a Peltier element with a thermal time constant of up to several seconds or the injection current with a characteristic modulation frequency that can reach several megahertz [14].

Two tunable laser spectroscopic techniques are the most widespread: one of them is based on direct detection, and the other, on laser frequency modulation. In the case of direct-detection spectroscopy, one or a few spectral absorption lines in a narrow spectral range are scanned by linearly varying the injection current of a laser diode, which leads to a linear output wavelength tuning. With increasing injection current, the laser output power increases and, as a result, the received signal also increases. Thus, absorption lines of the substance under study produce dips on the linearly rising signal. Quantitatively, the transmission function of a gas sample can be determined by normalising the signal to the shape of the injection current applied to the laser chip, which determines the shape of the spectral continuum in the absence of absorption (baseline). To solve the inverse problem, i.e. to find gas concentration, the Levenberg–Marquardt spectral fitting algorithm is often used in this approach [15]. Note that the major source of uncertainty in the solution is baseline uncertainty.

The other widely used technique – wavelength-modulation laser spectroscopy – involves high-frequency injection current modulation, which leads to a harmonic variation of the laser wavelength with time. This technique allows one to eliminate problems related to the baseline because the signal received by the photodetector has zero baseline. Moreover, using a synchronous detector as a receiver, one can raise the signal-to-noise ratio by more than one order of magnitude in comparison with direct detection results [16]. For adequate operation of this technique, the centre wavelength relative to which the laser wavelength is modulated should be stabilised to within 10^{-4} cm^{-1}. To achieve such a stabilisation level, the wavelength corresponding to the peak position of an absorption line of the gas under study should be used as a reference. However, in most cases emission wavelength modulation is limited to controlling the laser chip temperature with the use of a Peltier element, with no feedback to the laser wavelength relative to the position of the reference absorption line, which can ensure stabilisation accuracy only at a level of 10^{-2} cm^{-1} [17–20].

For modulation, use is made of a harmonic function, typically with a frequency from a few to tens of kilohertz. The signal received by the synchronous detector at the modulation frequency is proportional to the change in the incident laser power, which depends on wavelength. The demodulated signal at the modulation frequency, obtained by scanning the absorption line with modulated light, is similar in shape to the derivative of the profile of the absorption line.

To reduce the effect of the variation in laser output power corresponding to the modulated injection current, Schilt et al. [21] analysed the signal component at twice the modulation frequency, which had the shape of the second derivative of the line profile. This approach allows one to reduce the flicker noise in laser emission and the sensitivity of measurements to thermal fluctuations. These advantages allow for absorption measurements at a level from 10^{-7} to 10^{-6} with high-frequency wavelength modulation in the 10 MHz range [22]. One drawback to this technique is that calibration against known gas concentrations is needed.

In recent years, attempts were continued all over the world to make devices capable of detecting gas leaks and increased toxic gas concentrations in atmospheric air from an aerial vehicle. Some of them were terminated in the design stage. The other devices still have problems in ensuring parameters necessary for practical application: detection zone location accuracy, dynamic concentration range, maximum detection range, false detection probability minimisation, response

time, reliability, operational convenience, weight, size, and acceptable acquisition and maintenance costs.

The use of IR modulation spectroscopy also allows one to produce devices for remote detection of a particular gas and determination of its concentration [23–26]. However, existing devices are unsuitable for effective use in environmental monitoring from an aerial vehicle because of the insufficient level of laser wavelength locking to the peak position of a particular absorption line of the target gas or the absence of a stabilisation algorithm. Another problem limiting the utility of existing devices for remote sensing of the atmosphere is related to fluctuations in the phase difference between the received scattered laser light and the modulating signal due to changes in the optical path length to the scattering surface. As a result, it is impossible to use the standard synchronous detection scheme and, especially, commercial analog synchronous detectors, capable of recording only the fundamental and second signal harmonics.

It is worth noting an example of utilising a light-weight lidar system with digital interchange circuits, which is based on a diode laser and single-photon avalanche photodiode. Such an aerosol lidar system, employing a diode laser with a pulse energy of 1 μJ, without frequency stabilisation, was used to probe clouds over the Garabashi Glacier near the summit of Mount Elbrus at a distance of 4060 m with a signal-to-noise ratio of 225. However, this instrument is only intended for investigation of aerosols and is unsuitable for detecting minor atmospheric air components [27].

For remote detection of a particular gas and determination of its concentration, the principle of cross-correlation spectroscopy is used [28] along with modulation spectroscopy. This approach allows one to reach high sensitivity (at a level of 100 ppm m) in gas concentration measurements at a 100-m separation between the device and the surface that scatters the laser light. However, because of its large dimensions (600 × 600 × 250 mm) and weight (22 kg) and high energy consumption (200 W), the device should be mounted on board a piloted aircraft. Moreover, an operator monitoring the operation of the device with the use of a mobile computer for data processing should be present on board the aircraft.

The above-mentioned difficulties in remote sensing of atmospheric air for detection of a particular gas can be eliminated by using the technique proposed in this work, which relies on wavelength-modulation laser spectroscopy in combination with quadrature detection of the scattered light.

3. Experimental setup

Methane is an important indicator of the greenhouse effect and chemical reactions involving organic compounds and is widely used as an energy source. Good possibilities for detecting and observing leaks of natural gas or landfill gas, containing more than 50% methane, are offered by recent advances in unmanned aircraft engineering. For this reason, it is this component of atmospheric air which is chosen as a target gas for testing the proposed technique, which underlies the operation of an industrial pollution monitoring lidar system suitable for mounting on board an unmanned aerial vehicle (UAV). The possibility of mounting a device on board a UAV is an important economic factor for its potential applications in environmental monitoring or control over engineering processes, e.g. for detecting leaks in gas pipelines. The use of UAVs is more economically reasonable in comparison with manned aircraft.

The absorption lines of methane in the range 3.1–3.6 μm (2800–3200 cm^{-1}) are about two orders of magnitude stronger than those near 1.65 μm (6050 cm^{-1}), which is compensated for by the possibility of using, in the near-IR spectral region, inexpensive and compact InGaAs-based semiconductor photodiodes, whose sensitivity is higher than that of mid-IR photodetectors, also by two orders of magnitude.

The proposed approach to remote measurements of atmospheric gas concentrations, as exemplified by methane, can be realised by constantly measuring the intensity of an absorption line of this gas. Since the technique adequately works in the case of an isolated spectral line, the R4 line in the first overtone band $2\nu_3$ at a wavelength of 1.651 μm was used in our measurements. The full width at half maximum (FWHM) γ of the R4 absorption line at atmospheric pressure is ~0.15 cm^{-1}. This line does not overlap with absorption lines of H_2O and can be observed under medium and high humidity conditions. Therefore, an optimal laser source for the proposed approach is a semiconductor diode laser emitting near 1.65 μm. The wavelength of such a laser can be rapidly tuned around the peak position of the absorption line in question by modulating the injection current. The temperature of the chip can then be stabilised at a level of 10^{-4} K, which corresponds to a frequency control accuracy of ~10^{-4} cm^{-1} in the spectral range chosen.

Since the standard velocity of UAVs is 50–70 km h^{-1} and the spatial resolution of probing should be 1 m or better, a technique permitting sampling rates from 10 to 100 kHz is needed for resolving the problem under consideration. Moreover, its sensitivity should enable determination of methane excesses over the natural background from a few to tens of percent. A typical methane concentration in atmospheric air is 1.6 ppm. For a distance of 100 m, corresponding to twice a height of 50 m over the Earth's surface, we obtain 160 ppm m. As shown below, such requirements are met by the proposed technique, which relies on the use of modulation laser absorption spectroscopy and quadrature detection of light scattered by a surface.

To test the technique, we made a laboratory-scale prototype, schematised in Fig. 2. The light source used was a LasersCom DFB diode laser (DL) with a centre wavelength of 1.65 μm, emission bandwidth of 500 kHz, and temperature tuning range of 50 cm^{-1}. The laser package contained a Peltier thermoelectric element (for precision control over the temperature of the laser chip), thermistor, and monitor photodiode. The pump current of the laser was modulated sinusoidally, with a dc component of 100 mA. The modulation amplitude was calculated from the FWHM of the absorption line of methane and the modulation index (the ratio of the modulation amplitude to the absorption linewidth of the gas), which was taken to be 2.2 in order to maximise the wanted signal reconstructed from the Lorentzian profile of the line [29]. The modulation frequency f was 50 kHz.

At the output fibre pigtail of the laser, an optical isolator was placed, which was in turn connected to a fibre coupler. The optical coupling ratio was 9/1, so most of the light arrived at the analytical channel, and the rest was sent to the reference channel. In the analytical channel, the output collimating optics directed the laser beam, which was scattered by a scattering screen and collimated by the input optics of the photodetector module through a methane leak imitation in the surrounding air. The distance to the scattering screen, l, was

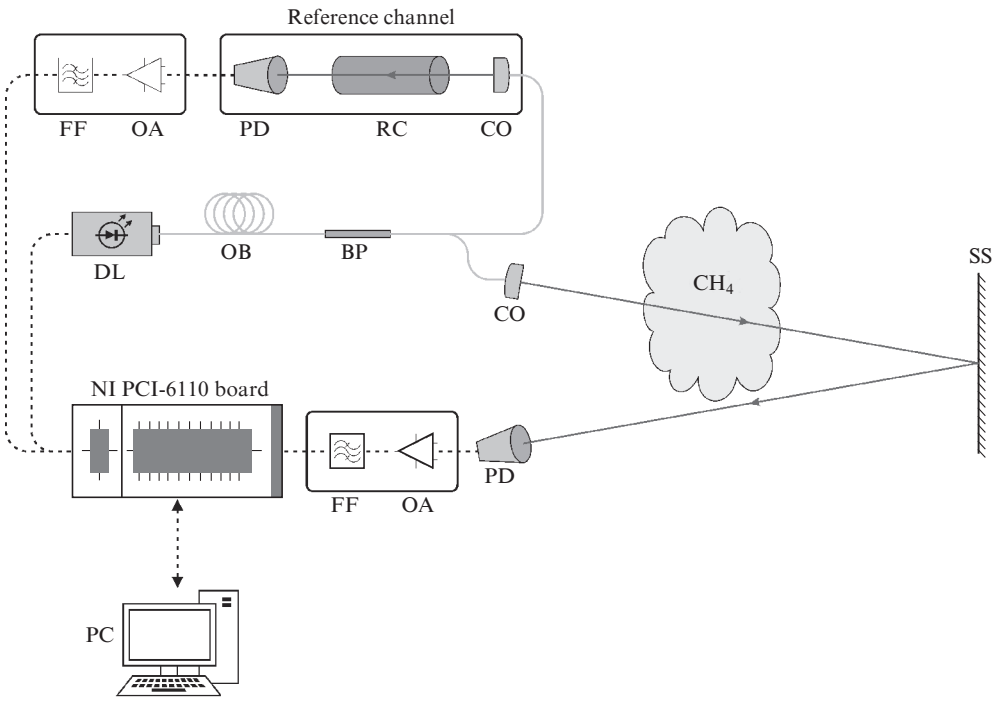

Figure 2. Schematic of the experimental setup: (DL) diode laser; (OF) optical fibre; (FC) fibre coupler; (CO) collimating optics; (SS) scattering screen; (RC) reference gas cell; (PD) photodetector; (OA) operational amplifier; (FF) band-pass frequency filter; (PC) personal computer.

6.3 m. The input optics had the form of a standard Thorlabs plano-convex lens of diameter $d = 51.2$ mm, with a near-IR anti-reflection coating. At the focus of the lens was located a Hamamatsu G8370-82 photodiode, with a photosensitive area 2 mm in size, which converted incident light to a photocurrent. The photocurrent was fed to a two-stage preamplifier comprising an operational amplifier and a band-pass frequency filter, with an equivalent transimpedance gain of 75 MΩ and a pass band from 50 to 150 kHz. Next, the analog signal was acquired by a 12-bit ADC of a National Instruments (NI) PCI-6110 board.

The reference channel, necessary for laser wavelength locking to the peak position of the absorption line of methane chosen, contained a collimator, which directed laser light through a cell filled with methane at a pressure of 10 mbar to a Hamamatsu G8370-81 photodiode, with a 1-mm photosensitive area. The reference channel signal also passed through a two-stage preamplifier with a pass band from 50 to 150 Hz and was read by another, independent, 12-bit ADC of the NI PCI-6110.

The laboratory-scale prototype lidar system was controlled using a personal computer and software written in the LabVIEW programming environment, which made it possible to control the drive current of the diode laser and the Peltier thermoelectric element with the help of the 16-bit DAC of the NI PCI-6110, record the signals from the monitor photodiode and thermistor of the laser, and analyse the data in real time.

4. Measurement technique

According to the Lambert–Beer law, in the case of a homogeneous gaseous medium, methane concentration c, and optical path length l, the transmittance T for a monochromatic laser beam that passed through a methane cloud can be represented as

$$T(\nu) = \exp[-\alpha(\nu)cl], \tag{1}$$

where $\alpha(\nu)$ is the absorption cross section of methane, whose variation with wavelength is determined by the profile of the line. In the lower atmosphere, collisional broadening of spectral lines prevails, so the lines have a Lorentzian profile:

$$f_{\mathrm{L}}(\nu) = \frac{\gamma^2}{\gamma^2 + (\nu - \nu_{\mathrm{cent}})^2}, \tag{2}$$

where γ is the FWHM of the spectral line; ν is the emission frequency; and ν_{cent} is the centre frequency of the line. The absorption cross section can then be represented in the following form:

$$\alpha(\nu) = \frac{\gamma^2}{\gamma^2 + (\nu - \nu_{\mathrm{cent}})^2}\alpha_0, \tag{3}$$

where $\alpha_0 = S/(\pi\gamma)$ is proportional to the intensity S of the spectral line.

For an optically thin medium, we have $\alpha(\nu)l \ll 1$ [at $l =$ 100 m and the natural methane concentration in atmospheric air, $\alpha(\nu_{\mathrm{cent}})l = 7 \times 10^{-3}$] and transmittance is given by

$$T(\nu) = 1 - \alpha(\nu)cl = 1 - \frac{\gamma^2}{\gamma^2 + (\nu - \nu_{\mathrm{cent}})^2}\alpha_0 cl. \tag{4}$$

The emission frequency ν of the semiconductor laser used as a light source is a function of temperature and drive current. In

the case of a sinusoidal injection current modulation, which ensures wavelength scanning across the spectral line near its peak position (at a frequency $\omega = 2\pi f$ and constant temperature), the instantaneous frequency ν and intensity I of the laser output can be represented as follows:

$$\nu(t) = \nu_0 + \Delta\nu\cos(\omega t), \tag{5}$$

$$I(t) = I_0 + \Delta I\cos(\omega t + \varphi), \tag{6}$$

where φ is the difference between the frequency and intensity modulation phases. The laser emission intensity modulation amplitude is taken to be proportional to the injection current modulation amplitude, which is valid for most practical purposes [30]. Transmittance (4) can be Taylor expanded at point ν_0. It can then be represented to second order in $\Delta\nu$ as follows:

$$T(\nu) = T_0 + T_1\Delta\nu\cos(\omega t) + T_2\frac{\Delta\nu^2}{4}[1 + \cos(2\omega t)], \tag{7}$$

where

$$T_0 = 1 - \frac{\gamma^2}{\gamma^2 + (\nu_0 - \nu_{\text{cent}})^2}\alpha_0 cl; \tag{8}$$

$$T_1 = \frac{2\gamma^2(\nu_0 - \nu_{\text{cent}})}{[\gamma^2 + (\nu_0 - \nu_{\text{cent}})^2]^2}\alpha_0 cl; \tag{9}$$

and

$$T_2 = \frac{2\gamma^2[\gamma^2 - 3(\nu_0 - \nu_{\text{cent}})^2]}{[\gamma^2 + (\nu_0 - \nu_{\text{cent}})^2]^3}\alpha_0 cl. \tag{10}$$

Using phase-sensitive synchronous detection, we can obtain signals proportional to T_1 and T_2. It is seen in Fig. 3 that, if the centre frequency ν_0 of the laser output coincides with the ν_{cent} of the absorption line of methane, the coefficient T_0, reproducing the shape of the transmittance, passes through a minimum (Fig. 3a); the coefficient T_1, corresponding to the signal at the modulation frequency f, becomes equal to the baseline level (Fig. 3b); and the magnitude of the coefficient T_2, corresponding to twice the modulation frequency, $2f$ (Fig. 3b), passes through a maximum.

Let K be the loss coefficient over the entire optical path length (from the light source to the photodetector). The intensity of the light incident on the photodetector can then be represented as follows:

$$P = KIT = K[I_0 + \Delta I\cos(\omega t + \varphi)] \times\left[T_{02} + T_1\Delta\nu\cos(\omega t) + T_2\frac{\Delta\nu^2}{4}\cos(2\omega t)\right], \tag{11}$$

where $T_{02} = T_0 + T_2\Delta\nu^2/4$. The term $P(\omega)$, varying at frequency ω, can be represented as

$$P(\omega = 2\pi f) = K[T_{02}\Delta I\cos(\omega t + \varphi) + T_1 I_0\Delta\nu\cos(\omega t)]. \tag{12}$$

It follows from (12) that the components of the signal intensity $P(\omega)$ at the modulation frequency differ in phase. If the centre frequency ν_0 of the laser output coincides with the ν_{cent} of the line, from the condition of an optically thin medium we obtain $T_{02} = 1$ and

$$P(\omega) = K[\Delta I\cos(\omega t + \varphi)]. \tag{13}$$

The maximum contribution of the signal intensity at the modulation frequency is then

$$P_{\max}(\omega) = K\Delta I. \tag{14}$$

In the case of synchronous detection of the signal at the doubled frequency 2ω, the signal intensity can be written in the form

$$P(2\omega = 2\pi 2f) = K\left[I_0 T_2\frac{\Delta\nu^2}{4}\cos(2\omega t)\right]. \tag{15}$$

At $\nu_0 = \nu_{\text{cent}}$, we obtain

$$P(2\omega) = KI_0\frac{\Delta\nu^2}{2\gamma^2}\alpha_0 cl. \tag{16}$$

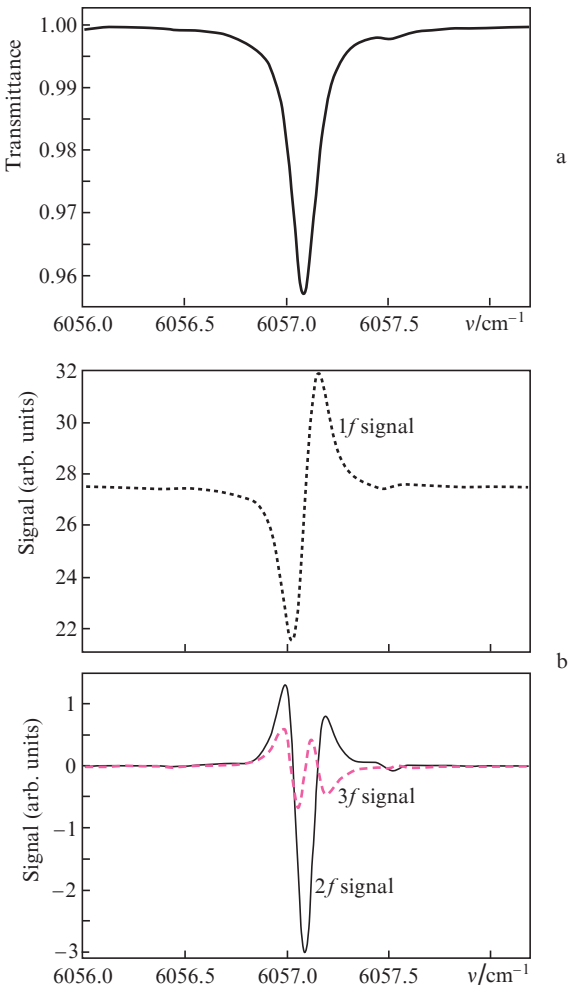

Figure 3. (a) Transmittance of methane (evaluated from HITRAN data) near the R4 line (centre wavelength of 1.651 μm) at a methane content of 1000 ppm m; (b) simulation results on the shape of harmonics of a signal that passed through a methane cloud (1000 ppm m) in atmospheric air, at the modulation frequency f and frequencies $2f$ and $3f$.

From (14) and (16), we find

$$\frac{P(2f)}{P(f)} = \frac{P(2\omega)}{P(\omega)} = \frac{\Delta\nu^2 I_0}{2\gamma^2 \Delta I}\alpha_0 cl. \tag{17}$$

Thus, from the ratio of the signals at the modulation frequency f and the doubled frequency $2f$ we can find the concentration of the gas being detected:

$$c = \frac{2\gamma^2\Delta I}{\Delta\nu^2 I_0}\frac{1}{\alpha_0 l}\frac{P(2f)}{P(f)} = \frac{2\gamma^2\Delta I}{\Delta\nu^2 I_0}\frac{\pi\gamma}{Sl}\frac{P(2f)}{P(f)}, \tag{18}$$

where the intensity of the spectral line, S, is 1.52×10^{-21} cm mol^{-1} for the R4 line.

To avoid a negative effect of modulation phase fluctuations on the level of the received signal, which can lead to an order of magnitude or larger error in concentration, the principle of quadrature detection was used in data processing [31–33].

The photodiode current in the analytical channel, amplified and transmitted through a frequency filter with a pass band $f - 2f$, is converted to a voltage, V_{in}, which is fed to the ADC. Since the buffer of the DAC and ADC is intended for N sinusoid periods, the first processing step is averaging over N periods:

$$V_{\text{in}}^{\text{av}} = \frac{1}{N}\sum_{i=1}^{N} V_{\text{in}}^{i}, \tag{19}$$

where V_{in}^{i} is the signal in the ith period. To restore the modulated signal, it is necessary to get rid of the baseline of the received signal:

$$V_{\text{in}}^{f} = V_{\text{in}}^{\text{av}} - \frac{1}{K_{\text{p}}}\sum_{k=1}^{K_{\text{p}}} V_k^{\text{av}}, \tag{20}$$

where V_k^{av} is the kth data point in the array of received signals averaged over N periods and K_{p} is the number of data points per sinusoid period. The subtraction of the baseline, connected with the constant term in the signal, can also be performed using a band-pass frequency filter. The cosine and sine components of the harmonic term in the signal at frequency nf and an instantaneous LD emission frequency ν are

$$S_{nf}^{\cos} = \sum_{k=1}^{K_{\text{p}}} V_k^{f}\cos(n\omega t_k), \tag{21}$$

$$S_{nf}^{\sin} = \sum_{k=1}^{K_{\text{p}}} V_k^{f}\sin(n\omega t_k), \tag{22}$$

where V_k^{f} is the kth data point in the array V_{in}^{f}. The magnitude of the harmonic component of the signal at frequency nf and instantaneous LD emission frequency ν (S_{nf}) is then given by

$$S_{nf} = \sqrt{(S_{nf}^{\cos})^2 + (S_{nf}^{\sin})^2}. \tag{23}$$

In this way, we can determine the harmonic components of the received signal at frequencies f, $2f$, and $3f$. Note that, in the absence of spectral features in the spectral region being scanned, the signal intensities at frequencies $2f$ and $3f$ are zero. The component at frequency f allows the total intensity of the received signal to be estimated, and from the $2f$ signal we can estimate the intensity of the line chosen. Because of this, as shown above, from the ratios of the signal components at frequencies $2f$ and f we can determine the concentration of the gas of interest when the centre frequency of the LD (ν_0) coincides with the peak position of the absorption line (ν_{cent}). Moreover, from the ratio of the sine and cosine components of the signal at the modulation frequency f we can determine the phase change $\Delta\varphi$ over the optical path length l, which in turn allows the distance to the light scattering surface to be found:

$$\Delta\varphi = \arctan\left(\frac{S_f^{\cos}}{S_f^{\sin}}\right), \tag{24}$$

$$l = \frac{c\Delta\varphi}{2\pi f} = \frac{1}{2\pi}\arctan\left(\frac{S_f^{\cos}}{S_f^{\sin}}\right)\frac{c}{f}. \tag{25}$$

The fundamental harmonic of the signal is shifted from zero, which is due to the residual amplitude modulation of the laser light. The asymmetry of the $2f$ and $3f$ signals is also due to the amplitude modulation [34]. The harmonic component at frequency $3f$ is not shifted, which makes it better suited for implementing the laser diode temperature stabilisation algorithm. Such stabilisation is necessary in systems operating in a wide dynamic range of backscattered signals [35].

In connection with this, the signal in the reference channel is processed in a similar manner, which makes it possible to continuously implement, using the third harmonic, the algorithm of laser diode temperature stabilisation to within 10^{-4} cm^{-1} to the zero position of the $3f$ signal, corresponding to the peak position of the spectral absorption line.

5. Experimental results

As mentioned above, to test the technique with the use of a laboratory-scale prototype we chose the R4 spectral absorption line of methane, at a wavelength of 1.651 μm. Figure 3a shows the transmittance of this gas calculated using HITRAN data and corresponding to a methane concentration in atmospheric air over the optical path length of laser light at a level of 1000 ppm m.

For the spectral line chosen, we modelled the propagation of laser light emitted by the DL at a constant injection current of 100 mA and current modulation amplitude of 9 mA, with the temperature stabilised using the R4 line, subsequent light scattering by a screen located a distance $l = 6.3$ m from the collimating lens of diameter $d = 51.2$ mm, and signal processing. As a result of model signal processing, we obtained calculated harmonics of the signal at the modulation frequency f, doubled frequency $2f$, and tripled frequency $3f$. The shapes of the resultant f, $2f$, and $3f$ components of the signal are shown in Fig. 3b.

Using the temperature tuning of the laser wavelength, we scanned the transmittance around the R4 line at the same experimental parameters: DL injection current, distance to the scattering screen, input optical channel aperture, and methane concentration in atmospheric air. The signal obtained by such scanning was processed as described in Section 4. Figure 4 shows the shape of the ratio of the harmonics of the signal at frequencies f and $2f$, calculated as a result of data processing during the experiment. Also pre-

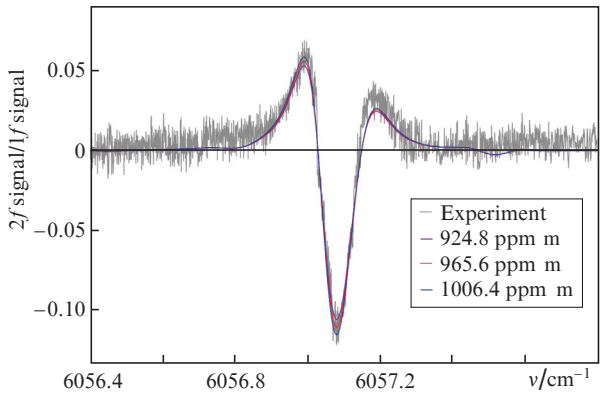

Figure 4. (Colour online) Ratio of the harmonics of the signal at frequency $2f$ and the modulation frequency f. Experimental data and simulation results for methane contents of 924.8, 965.6, and 1006.4 ppm m.

sented in Fig. 4 are simulation results on the ratio of signals at frequencies $2f$ and f and methane contents of 924.8, 965.6, and 1006.4 ppm m in atmospheric air for experimental data interpretation.

The possible contribution of the residual amplitude modulation of the signal was left out of account in simulation, which led to a deviation of the experimentally determined ratio of the $2f$ signal to the $1f$ signal from the simulation results at high frequencies. At the same time, it is seen from Fig. 4 that this approach makes it possible to assess the accuracy of the model from the noise track of the measured signal, associated with the inherent noise of the photodetector, the digital noise of the NI PCI-6110, and DL intensity noise. The contribution of flicker noise, characteristic of laser spectroscopy, is missing in this case owing to the technique used and the presence of a band-pass frequency filter in the signal detection/amplification module.

A solution to the inverse problem is the methane concentration evaluated using particular $1f$ and $2f$ signals and Eqn (18). As seen from Fig. 4, we can then find the target gas concentration for experimentally determined harmonic components:

$$c_{\text{exp}} = (4.44 \pm 0.19) \times 10^{17} \text{ mol cm}^{-3}. \quad (26)$$

For a 5.44-cm-long methane-containing zone in atmospheric air at a temperature of 25 °C and atmospheric pressure, this corresponds to 965.6 ± 40.8 ppm m. The methane concentration in the measuring channel, as determined with an Inficon DI200 pressure sensor, was $c = (4.6 \pm 0.1) \times 10^{17}$ mol cm^{-3}, which corresponded to 1000.6 ± 23.2 ppm m. Thus, the difference between the average experimentally determined gas concentration and the actual methane concentration, i.e. the error of the model used, was 3.5%.

To assess the sensitivity of the laboratory-scale prototype, we chose a methane content of 1000 ppm m in atmospheric air. Using the above parameters of the setup and averaging the signal over 2 ms, which corresponded to the number of averaging steps $N = 100$, we found the standard deviation (STD) of the signal and its average over 50 sequential values of the ratio of the $2f$ and $1f$ signals, which allowed us to assess the sensitivity D of the laboratory-scale prototype at a total operation time of 100 ms,

$$D = c\frac{N}{\sum_i^N S_{2f}/S_{1f}}\text{STD}[S_{2f}/S_{1f}]_N = 42 \text{ ppm m}, \quad (27)$$

which corresponds to 26% of 160 ppm m (background methane content of 1.6 ppm over an optical path length of 100 m). For comparison, one commercial gas sensor [28] for use on board manned aircraft because of its large size and weight has a sensitivity of 25 ppm m for signal averaging over 500 ms.

Estimates show that increasing the diameter of the receiving optics to 100 mm, improving parameters of the band-pass filter, and replacing the NI PCI-6110 by electronics under development for a field instrument with allowance for the increase in the distance from the instrument to the scattering surface up to 50 m should improve the sensitivity of the instrument by about a factor of two relative to that obtained for the laboratory-scale prototype at $l = 6.3$ m. Further, to improve the sensitivity of the field instrument we envisage the use of a fibre amplifier of laser light.

6. Conclusions

We have presented results of the operation of a laboratory-scale prototype of an instrument based on the use of wavelength-modulation laser absorption spectroscopy in combination with quadrature signal detection. It has been shown that, at characteristic distances of tens of metres, the prototype compares well in attainable sensitivity level (tens of ppm m) to existing devices of an analogous class. Moreover, the weight and energy consumption of an instrument based on the proposed principles correspond to useful load characteristics of existing UAVs. Subsequently, in designing a compact lidar-based field gas analyser, we plan to switch to control electronics based on a microcontroller and FPGA with fast ADCs and DACs, increase the diameter of the receiving optics, and improve the performance of the band-pass frequency filter in the input module of the analytical channel of the instrument. We plan to mount the instrument on board a UAV, which will appreciably simplify and cheapen detection of leaks in gas pipelines and monitoring of air near hazardous production facilities and landfill sites.

Acknowledgements. This work was supported by the Russian Foundation for Basic Research (Grant No. 18-29-24204).

References

1. Allen M.G. *Meas. Sci. Technol.*, **9** (4), 545 (1998).
2. Laj P., Klausen J., Bilde M., Plass-Duelmer C., Pappalardo G., Clerbaux C., Coheur P. *Atmos. Environ.*, **43** (33), 5351 (2009).
3. Ponurovskii Y.Y., Zaslavskii V.Y., Nadezhdinskii A.I., Spiridonov M.V., Stavrovskii D.B., Shapovalov Y.P., Petrenko Y.M. *Biophysics*, **64** (6), 870 (2019).
4. Wunch D., Toon G.C., Blavier J.-F.L., Washenfelder R.A., Notholt J., Connor B.J., Wennberg P.O. *Philos. Trans. R. Soc., A*, **369** (1943), 2087 (2011).
5. Williams D.E., in: *Solid State Gas Sensors* (Adam Hilger Series on Sensors) (Bristol: IOP Publ., 1987) p. 71.
6. Bakker E., Telting-Diaz M. *Anal. Chem.*, **74** (12), 2781 (2002).
7. Lackner M. *Rev. Chem. Eng.*, **23** (2), 65 (2007).
8. Eng R., Butler J., Linden K. *Opt. Eng.*, **19** (6), 196945 (1980).
9. Zenevich S.G., Klimchuk A.Yu., Semenov V.M., Spiridonov M.V., Rodin A.V. *Quantum Electron.*, **49** (6), 604 (2019) [*Kvantovaya Elektron.*, **49** (6), 604 (2019)].

10. Nadezhdinsky A.I., Ponurovsky Y.Y., Shapovalov Y.P., Popov I.P., Stavrovsky D.B., Khattatov V.U., Kuzmichev A.S. *Appl. Phys. B*, **109** (3), 505 (2012).
11. Faist J., Capasso F., Sivco D., Sirtori C., Hutchinson A., Cho A. *Science*, **264** (5158), 553 (1994).
12. Szweda R. *Diode Laser Materials and Devices – A Worldwide Market and Technology Overview to 2005* (Elsevier, 2001).
13. Sandström L., Bäckström S., Ahlberg H., Höjer S., Larsson A. *Infrared Phys. Technol.*, **39** (2), 69 (1998).
14. Lackner M., Totschnig G., Winter F., Ortsiefer M., Amann M., Shau R., Rosskopf J. *Meas. Sci. Technol.*, **14** (1), 101 (2002).
15. Hennig O., Strzoda R., Mágori E., Chemisky E., Tump C., Fleischer M., Eisele I. *Sens. Actuators, B*, **95** (1-3), 151 (2003).
16. Jung E., Kim T., Song K., Kim C. *Spectrosc. Lett.*, **36** (1-2), 1670 (2003).
17. Li H., Rieker G., Liu X., Jeffries J., Hanson R. *Appl. Opt.*, **45** (5), 1052 (2006).
18. Rieker G., Jeffries J., Hanson R. *Appl. Opt.*, **48** (29), 5546 (2009).
19. Sun K., Chao X., Sur R., Goldenstein C., Jeffries J., Hanson R. *Meas. Sci. Technol.*, **24** (12), 125203 (2013).
20. Mei L., Svanberg S. *Appl. Opt.*, **54** (9), 2234 (2015).
21. Schilt S., Thevenaz L., Robert P. *Appl. Opt.*, **42** (33), 6728 (2003).
22. Schiff H., Mackay G., Bechara J. *Res. Chem. Intermed.*, **20** (3-5), 525 (1994).
23. Iseki T., Tai H., Kimura K. *Meas. Sci. Technol.*, **11** (6), 594 (2000).
24. Carvalho J., Lehmann H., Bartelt H., Magalhães F., Amezcua-Correa R., Santos J., Knight J. *J. Sens.*, **2009**, 398403 (2009).
25. Engelbrecht R. *Spectrochim. Acta, Part A*, **60** (14), 3291 (2004).
26. Frish M., Wainner R., Stafford-Evans J., Green B., Allen M., Chancey S., Wehnert P., in *Photonic Applications Systems Technologies Conference* (OSA, 2005) p. JThF3.
27. Pershin S.M., Grishin M.Y., Zavozin V.A., Lednev V.N., Lukyanchenko V.A., Makarov V.S. *Laser Phys. Lett.*, **17** (2), 026003 (2020).
28. Ershov O.V., Klimov A.G., Vavilov V.P. *Quant. InfraRed Thermogr. J.*, **3** (1), 41 (2006).
29. Reid J., Labrie D. *Appl. Phys. B*, **26** (3), 203 (1981).
30. Cassidy D., Reid J. *Appl. Opt.*, **21** (7), 1185 (1982).
31. McGettrick A.J., Duffin K., Johnstone W., Stewart G., Moodie D.G. *J. Lightwave Technol.*, **26** (4), 432 (2008).
32. Upadhyay A., Lengden M., Wilson D., Humphries G.S., Crayford A.P., Pugh D.G., Johnstone W. *IEEE Photonics J.*, **10** (6), 1 (2018).
33. Leis J., Martin P., Buttsworth D. *Electron. Lett.*, **48** (5), 259 (2012).
34. Liu J., Jeffries J., Hanson R. *Appl. Phys. B*, **78** (3-4), 503 (2004).
35. Van Well B., Murray S., Hodgkinson J., Pride R., Strzoda R., Gibson G., Padgett M. *J. Opt. A: Pure Appl. Opt.*, **7** (6), S420 (2005).